Science of the Total Environment 883 (2023) 163707

Contents lists available at ScienceDirect

Science of the Total Environment

journal homepage: www.elsevier.com/locate/scitotenv

Estimating mussel mound distribution and geometric properties in coastal salt marshes by using UAV-Lidar point clouds

Daniele Pinton [a,*], Alberto Canestrelli [a], Sydney Williams [b], Christine Angelini [b], Benjamin Wilkinson [c]

[a] Department of Civil and Coastal Engineering, University of Florida, PO Box 116580, Gainesville 32611, FL, USA
[b] Department of Environmental Engineering Sciences, University of Florida, PO Box 116580, Gainesville 32611, FL, USA
[c] School of Forest Resources and Conservation, University of Florida, PO Box, Gainesville 32611, FL, USA

HIGHLIGHTS

- A detection algorithm has been created to identify mussel mounds from point clouds.
- The classifier distinguishes mounds from non-mounds sites with an accuracy of 95 %.
- The algorithm gives the distribution, height, radius, volume and distance of mounds.
- The mounds volume corresponds to an addition to the average marsh elevation of 7 mm.
- The algorithm can be used to promote marsh conservation and enhancement projects.

GRAPHICAL ABSTRACT

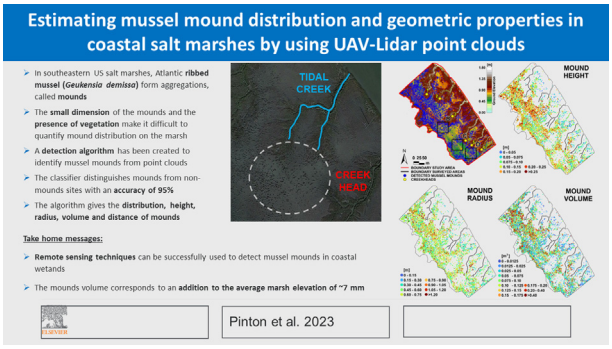

ARTICLE INFO

Editor: Martin Drews

Keywords:
Salt marshes
Remote sensing
Unmanned Aerial Vehicle (UAV)
Light Detection and Ranging (Lidar)
Green infrastructure
Coastal restoration
Random Forest
Mussel mounds
Ribbed mussels
Geukensia demissa

ABSTRACT

The Atlantic ribbed mussel (*Geukensia demissa*) is common in southeastern US salt marshes, where they form dense aggregations (mounds), that occur in the highest densities and sizes on the marsh platform close to the tidal creeks' heads. Within these marshes, mussels help build marsh elevation via their biodeposition of organic and inorganic material, stimulate the growth of the dominant foundation species cordgrass (*Spartina alterniflora*), and create hotspots of invertebrate biodiversity, nutrient cycling, and drought resilience. Given their powerful role, there is rising interest in assessing natural variation in the distribution of mussel mounds and using such information to guide marsh conservation and restoration strategies. However, gathering such information is challenging, because the small dimension (~1 m) of the mounds and the presence of overlying vegetation make it difficult to quantify mound distribution on the marsh. Therefore, this study presents a new procedure to compute the distribution, height, radius, volume, and distance of mounds in marsh environments using remote sensing. A high-resolution UAV-Lidar point cloud has been collected over a highly vegetated salt marsh in Georgia, USA, using a custom-built laser scanner system. An original detection algorithm, based on a Random Forest classifier, has been implemented to identify the mounds from the point cloud. The algorithm has been trained and tested on surveyed mounds and provides their location and geometric properties. Results indicate that the classifier can distinguish mussel mounds from non-mussel mound locations with an accuracy of 95 %. The classifier identified ~8000 mounds, which occupy 10 % of the study domain, and a volume (shells + feces/pseudofeces) of 680 m^3. The method is highly useful in efforts to monitor mussel mounds over time and scale up to assess mounds across sites, providing invaluable data for future studies related to the geomorphic evolution of marshes to sea level rise and siting marsh conservation and enhancement projects.

* Corresponding author.
E-mail addresses: daniele.pinton@ufl.edu (D. Pinton), alberto.canestrelli@essie.ufl.edu (A. Canestrelli), sydney.williams@ufl.edu (S. Williams), christine.angelini@essie.ufl.edu (C. Angelini), benew@ufl.edu (B. Wilkinson).

http://dx.doi.org/10.1016/j.scitotenv.2023.163707
Received 24 December 2022; Received in revised form 7 March 2023; Accepted 20 April 2023
Available online 25 April 2023

1. Introduction

Consistent coastal wetland loss has been documented in the past several decades (Li et al., 2018), including progressive transformations of salt marshes into tidal flats and open ocean areas. Examples of these transformations are the loss of ~10,230 km^2 of the coastal zone in Louisiana, USA between 1930 and 1990 (Boesch and Turner, 1984), the 70 % reduction of the salt marshes in the Venice Lagoon, Italy in the last 200 years (Brambati et al., 2003), and the ~81 % loss of coastal land in the Boston area (MA, USA) since 1777 (Kravchenko, 2009). Among the primary causes of marsh loss, sea-level rise (SLR, Reed, 1995) promotes the lateral expansion of the tidal network by increasing the tidal prism and, in turn, increasing sediment export from salt marsh systems (Pinton et al., 2022). SLR can also result in longer periods of tidal inundation, leading to marsh drowning, and consequently, their loss (Morris et al., 2002). The forecasted global coastal wetland response to SLR indicates a marsh loss rate of ~20–60 % during this century (Nicholls et al., 2007). Anthropogenic impacts, such as oil spills, land reclamation, and sediment reduction due to urbanization aggravate this trend (Warren et al., 2002; Brambati et al., 2003; Nicholls et al., 2007; Peteet et al., 2018).

Various efforts have been made to reverse or reduce this trend through gray and green (i.e., nature-based) infrastructures. Gray infrastructure represents traditional engineering, which uses hard constructions such as seawalls, breakwaters, dikes, or groins, to protect coastlines. Due to the high costs to maintain the long-term efficiency of man-made restoration approaches (Stagg and Mendelssohn, 2011), nature-based solutions have gained popularity. Green infrastructure uses natural materials, such as plants, reefs, sand, and ecosystem engineers to protect and enhance the resilience of coastal regions while maintaining natural shoreline processes. Many of these solutions strive to bolster and use bivalves, such as mussels and oysters, to enhance ecosystem services and resilience (Coen et al., 2007; Angelini et al., 2016; Gray et al., 2021).

Bivalves are ecosystem engineers that modify their environment via abiotic and biotic processes. They can mitigate soil erosion (Bertness, 1984; Angelini et al., 2015; Derksen-Hooijberg et al., 2018a; Crotty and Angelini, 2020) and enhance marsh resilience to environmental stress and disturbance (Nardin et al., 2021). They also remove nutrient-rich particulate from the water column via filter feeding and subsequently eject feces and pseudofeces (Bertness, 1984). Along the southeast Atlantic coast (USA), the Atlantic ribbed mussel, *Geukensia demissa* (Dillwyn), forms dense patches (hereafter, 'mussel mounds' or just 'mounds') distributed across higher elevation marsh platforms and especially around the heads of tidal creeks (see Fig. S.1 Supplementary Materials, Section S1) (Kuenzler, 1961; Crotty and Angelini, 2020). A portion of the sediments expelled from mussels contributes to the lateral and vertical growth of the mounds. The remaining portion is redistributed across marsh platforms over time, contributing to both accretion and land formation of the marsh (Smith and Frey, 1985; Crotty et al., 2023).

Mussels are commonly found in a mutualistic association with a salt marsh cordgrass, *Spartina alterniflora* (Bertness, 1984; Angelini et al., 2016). Mussels enhance cordgrass resistance to drought stress by increasing the water volume stored in the soil by 60 % and stimulate cordgrass growth by about 190 % (Angelini et al., 2016). Cordgrass, in turn, protects mussels from predation and thermal stress (Pennings and Bertness, 2001). Through this mutualism, both species enhance organic production, promote inorganic sediment trapping, and increase sediment stability (Pennings and Bertness, 2001). As a result of the growing literature showing the value and potential use of mussels in salt marsh resilience to drought and in driving patterns in sediment deposition, invertebrate diversity, and primary production, there is growing interest in more intentionally integrating mussels into salt marsh restoration or creation efforts (that currently focus on transplanting only cordgrass) as well as in identifying marshes for conservation (i.e., those that may be particularly resilient to sea level rise due to their relatively high densities of mussel mounds) and for marsh enhancement (i.e., potentially increasing mussel mound density to elevate the marsh's ability to resist droughts for keep pace with sea level rise). However, the development of a low-cost and accurate method to survey mussel mounds' geometry and distribution is needed to support the planning of such proactive marsh management measures.

Overall, traditional survey methods for mussel mounds are based on in situ observation, measurement, and data recording to estimate the distribution, abundance, and size of the mounds in a particular study area (Kuenzler, 1961; Julien, 2018; Moody and Kreeger, 2020). Measurements involve the use of instruments, such as measuring tapes, rulers, or GPS rovers to measure the geometry (i.e., diameter, height) of the mounds. Another method is to use a quadrat or transect survey, which involves placing a frame or line in the area of interest and counting the number of mounds within the quadrat or along the transect (Crotty et al., 2020). This method is useful to estimate the distribution and density of mounds in a particular study area. Cameras can also be used to document the size and shape of the mounds and to observe any associated flora or fauna. These approaches provide accurate data, but they damage the marsh by trampling, are time-consuming (both for collecting and processing the dataset), costly, and limited to easily accessible and relatively small study areas. One way to speed up the survey is to engage multiple operators in data collection. However, this approach can result in greater damage to the marsh. Therefore, there is a need for reliable remote sensing techniques that do not suffer these limitations.

Various remote sensing approaches have been used to characterize the habitat and demographics of mussel mounds. For instance, (Brockmann and Stelzer, 2008) and (Adolph et al., 2018) used aerial and satellite images, to monitor mussel beds (i.e., blue mussels, *Mytilus edulis*) in coastal areas. Additionally, (Julien, 2018) used a combination of airborne Light Detection and Ranging (Lidar) point clouds and field surveys to characterize mussels' habitat in coastal areas. However, this approach only gives a probability of occurrence of mussel mounds and does not provide their spatial distribution. The main aim of this paper is to develop a non-intrusive, flexible, and reliable method to map mussel mounds in the field, and get their geometrical characteristics (i.e., height, radius, and volume). This quantification is necessary since the spatial distribution and temporal evolution of mussel mounds are linked to changes in sedimentation rates and water quality. In particular, recent work showed how mussel mounds favor sediment trapping, marsh aggradation (Crotty et al., 2023), and coastal resilience (Angelini et al., 2016).

Unmanned Aerial Vehicles (UAVs) are becoming a standard technology used for various purposes, like high-resolution mapping (Meng et al., 2017), and shoreline surveys (Farris et al., 2019). When coupled with Lidar techniques, UAVs proved to be a valuable resource to describe the topography of highly vegetated areas like *Spartina alterniflora* salt marshes (Schmid et al., 2011; Schalles et al., 2013; Ali-Sisto and Packalen, 2017; Pinton et al., 2020b, 2020a, 2021).

Since mounds accrete vertically and enhance vegetation growth, they display a ground elevation, vegetation density, and vegetation height different from that of the surrounding marsh and are thus conducive for UAV-Lidar point cloud detection. To our knowledge, this approach has not been previously used to identify mussel mounds in estuarine environments.

2. Material, methods, and calculation

In this study, we implemented an original mound detection algorithm based on a Random Forest classifier. The model was trained and tested using the spatial location, and the geometric properties (i.e., height, radius, volume, and distance) of mussel mounds we collected on a highly vegetated *Spartina alterniflora* salt marsh located in Georgia, USA (Fig. 1).

The proposed model allows the detection of mussel mound distribution by using a combination of remote sensing and direct survey approaches. Since the classification algorithm require the spatial location (i.e., XY coordinates) of a limited number of mussel mounds (~40) to be trained, the collection of these points can be performed causing minimum damage to the marsh surface and vegetation. The points can be either identified by using satellite, airborne, or UAV imagery data, nullifying any damage to the

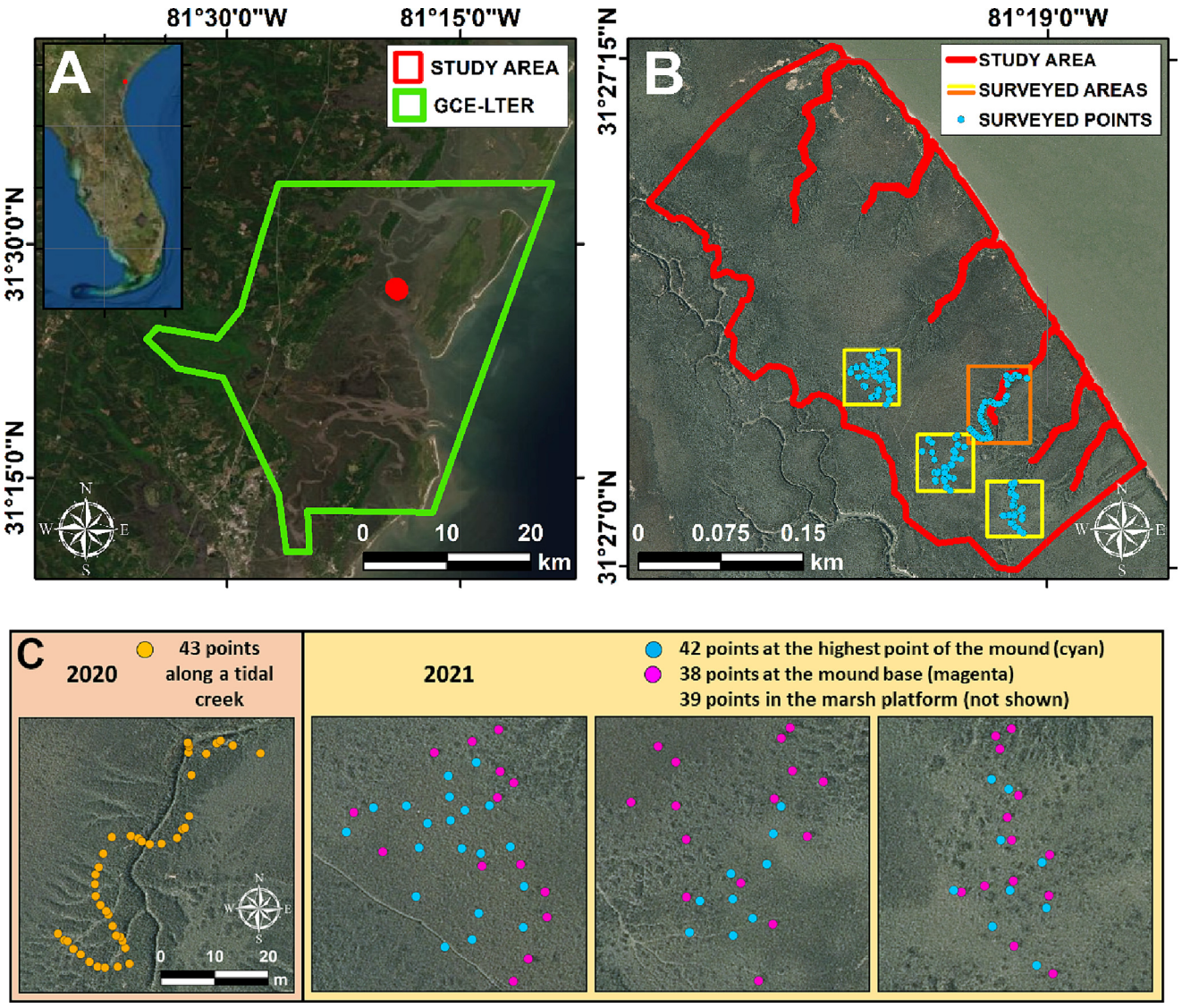

Fig. 1. (A-B) The geographic location of the study domain. The study area is a salt marsh in Georgia, USA, within the Georgia Coastal Ecosystem Long Term Ecological Research (GCE-LTER) domain. The Old Tea Kettle Creek, an 8-km-long tidal channel, flanks the marsh at its northeastern boundary. Six major tidal creeks cross the marsh. (C) Spatial distribution of the points surveyed in the study domain. The orange dots are the points collected in 2020 along a tidal creek. The cyan and magenta dots are the points collected in 2021 at the highest point and the base of the mussel mounds.

marsh system by making it a fully remote sensing approach. For these reasons, and because of the flexibility and velocity of remote sensing approaches, the proposed model can be transferred to other locations, and be used to perform multiple surveys on the same area, to study and track the evolution of the mussel mound distribution.

Our procedure to identify the location and the geometric properties of the mussel mounds in a salt marsh is described in the following sections and summarized in Fig. 2.

2.1. Study area

The study site is a ~0.1 km^2 portion of an estuarine salt marsh system, located in Georgia, USA, within the Georgia Coastal Ecosystem Long Term Ecological Research (GCE-LTER) domain. The marsh is flanked at its north-eastern boundary by Old Teakettle Creek, which is an 8-km-long tidal channel crossed by six creeks of various sizes and cross-sectional geometries that run almost perpendicular to the Old Teakettle (Fig. 1). Sediments and organic material are primarily delivered to the marsh platform by these fringing tidal creeks. The local tide has a semi-diurnal oscillation with a Mean High Water level of 1.073 m Above the Mean Sea Level (AMSL, NOAA tide gauge "Daymark #156, Head of Mud Creek, GA" #8674975). However, the water level can reach 1.5–2.0 m AMSL during spring tides, submerging the salt marsh with a water layer of ~1 m. *Spartina alterniflora* is the dominant macrophyte in this area (Hladik et al., 2013; Schalles et al., 2013). Its height and density depend on marsh topography and nutrient availability, both varying with distance from tidal creeks (Wiegert et al., 1983). For instance, short and medium *Spartina alterniflora* occupies the high marsh platform and have an average stem height of 0.20–0.60 m. Tall *Spartina alterniflora*, instead, fills the lower marsh and the creek banks with heights up to 2 m (Wiegert et al., 1983).

2.2. Datasets

2.2.1. UAV-Lidar detection and pre-processing

We collected a UAV-Lidar point cloud of the study domain, which area is ~0.1 km^2, in July 2019, during low tide, when the marsh was dry. Data were collected using a custom-built Lidar system, based on a Velodyne VLP-16 Puck Lite laser scanner mounted on a DJI Matrice 600 UAV. The flight was operated at a 40 m altitude with a 50 m flight line spacing. The wavelength of the Velodyne laser scanner was 903 nm. The density of the

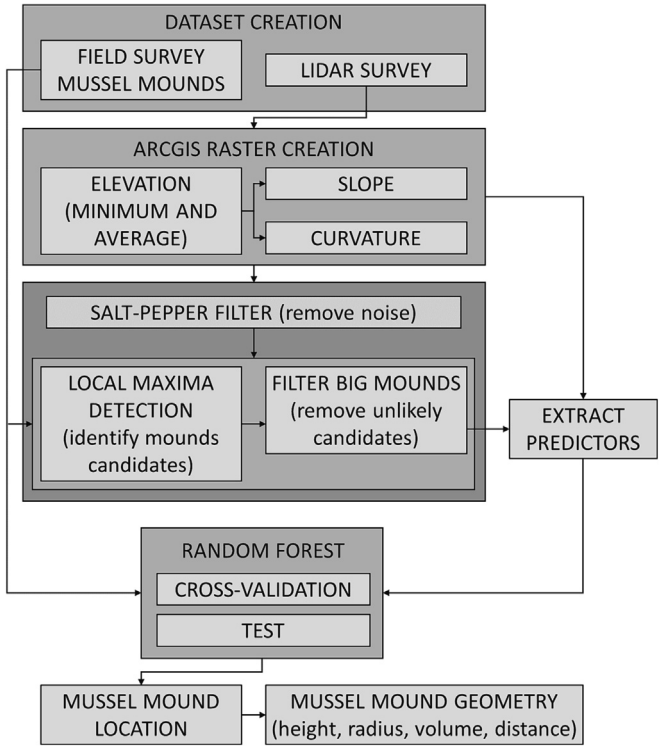

Fig. 2. Flow chart describing the procedure used in this study to identify the location and the geometric properties of the mussel mounds in a salt marsh.

resulting point clouds was ~130 points m^{-2} on average. Additional information is reported in the Supplementary Material, Section S2.1.

We applied two filters to the point cloud to remove the points lower than 0 m AMSL and higher than 2.50 m AMSL. The points below 0 m AMSL describe the surface of the Old Tea Kettle Creek. The points above 2.50 m AMSL describe birds and the upper part of the power line crossing the marsh. The lower part of the utility poles was removed manually.

2.2.2. Mussel mounds field surveys

A hundred and sixty-two plots were laid out and surveyed over the study area, at low tide, between August 2020 (43 plots) and April 2021 (119 plots), 13 and 21 months after the drone flight, respectively. Both datasets were collected after the drone survey to populate datasets used for a different research study (Crotty et al., 2023). Even if data collection was performed after the drone survey, this does not affect the results of our survey because: (i) the ground elevation (Z coordinate) is not used by our identification algorithm; (ii) the marginal error in the X and Y coordinate of the GPS-RTK point is smaller than the average dimension of a mussel mound (i.e., ~50 cm, according to the literature).

The points surveyed in 2020 were placed along a tidal creek in the study area (orange square in Fig. 1B), on the marsh platform devoid of mussels ("creek plots", orange dots in Fig. 1C). The plots collected in 2021 were placed at three different survey locations in the study area, between the central and lower part of the marsh (yellow squares in Fig. 1B). The three survey locations are on the marsh platform around the head of three different tidal creeks. Eighty of the points surveyed in 2021 were collected on the mussel mounds ("mound plots"), and the other 39 were on the mash platform devoid of mussels ("platform plot"). Forty-two of the mound plots were collected at the highest point of the mound ("mound top", cyan dots in Fig. 1C). The mound top is visually identified during the survey and generally corresponds to the center of the mound. The remaining 38 plots were collected at the mound base (magenta dots in Fig. 1C). Only 11 pairs of points, consisting of a top and a base plot, were surveyed on the same mound. The parameter surveyed at each plot was the geographic position of the plot center. The geographic survey was performed using an RTK-GPS (Trimble R6 GNSS ±2 cm vertical and ±1 cm horizontal accuracy). Fig. 1C contains a summary of the number of plots surveyed per each survey location.

2.3. Mussel mound recognition algorithm

We developed an algorithm that identifies the geographic position of the mussel mounds by using the predictors calculated from the collected UAV-Lidar point cloud.

The algorithm was based on the following steps, which are described in-depth in the sections below:

STEP 1. We calculated the spatial distribution of the ground elevation, slope, and curvature on the marsh at different spatial resolutions. Each spatial distribution constituted a distinct raster dataset.

STEP 2. Each ground elevation raster was filtered to remove noise and then used to determine the location of the local maxima. Each local maximum indicated a possible candidate for the central location of a mussel mound.

STEP 3. We considered the cells inside a circular 2.5-meter radius neighborhood around the maximum, and we average ground elevation, slope, and curvature at fixed radius intervals. This gave us the radial distribution of those quantities, that were used as predictors in STEP 4. We then computed the skewness of the radial distribution, and we defined the edge and base of the mound candidate, from which we computed the average slope in the radial direction.

STEP 4. We applied the procedure described in STEP 3 to the surveyed mounds to compute the predictors, which were used to train and test a Random Forest classifier. The tested classifier was then applied to the mound candidates obtained at STEP 2, to identify which of them were mussel mounds.

2.3.1. Ground elevation, slope, and curvature maps (STEP 1)

Here we identified possible candidates for the central location of a mussel mound. We first determined the spatial distribution of ground elevation, slope, and curvature in the marsh system, from the collected UAV-Lidar point cloud (STEP 1) by using the ArcGIS suite (ESRI. ArcGIS Desktop: Release 10.7).

Elevation maps were obtained by applying the "*LAS dataset to raster*" ArcGIS tool to the UAV-Lidar dataset. The tool generated a regular cell array that encompassed the UAV-Lidar dataset. We chose two different spatial resolutions (i.e., cell size) for the rasters, corresponding to 5 and 10 cm. For each resolution, we computed the minimum and average elevation of the points of the cloud which were contained in each cell (hereafter called "MinE" and "AveE", respectively), obtaining a total of four elevation rasters. We used these rasters based on the considerations outlined in Section S2.2 of the Supplementary Material. The tool used a void-fill method based on linear triangulation to assign a value to the cells that did not contain any point.

Slope and curvature maps were obtained by applying the corresponding ArcGIS tools (i.e., "*Slope*" and "*Curvature*", see Supplementary Material, Section S2.3) to each of the four elevation rasters.

2.3.2. Local maxima/candidate mounds identification (STEP 2)

We identified the cells containing a local ground elevation maximum, for each of the MinE and AveE elevation rasters. This was done by applying three consecutive filters to each raster. The first one was a gaussian smoothing filter and was used to remove salt and pepper noise (Das et al., 2015), and to enhance the shape of the mussel mounds, by flattening the surrounding marsh platform. The filter was based on a 7 cell × 7 cell gaussian kernel with a standard deviation of 17. This value was obtained from a sensitivity analysis. The second one was a local maxima detection filter, which identified the cells that were mussel mound candidates. A cell was a candidate if

its elevation was higher than the elevation of the eight surrounding cells. For each candidate, we then calculated an estimate of the mound height as the difference between the elevation of the candidate itself and the minimum elevation in a 21 cell × 21 cell stencil centered on the candidate. A third filter removed the candidate mound from the list if its height was not comprised between 2 and 35 cm (see Supplementary Material, Section S2.4).

2.3.3. Classification predictors from Lidar point cloud (STEP 3)

Here we list the classification predictors of our machine-learning algorithm. The predictors were calculated for the mussel mound candidates obtained in STEP 2, and for the surveyed mussel mounds.

The predictors were obtained from the spatial distribution of the ground elevation, slope, and curvature in the 2.5-meter radius area surrounding the centers of the surveyed and calculated mussel mounds. These distributions were calculated by averaging the values of the cells which center was contained in the annuluses (also known as circular crowns) centered in the local maxima cell identified in STEP 2 (Fig. 3A). The thickness of each annulus was chosen equal to the spatial resolution (5 or 10 cm) of the considered raster. This allowed us to obtain a relatively smooth profile of the mound (Fig. 3B). We then identified the mound edge and base as the locations, starting from the center of the mound, where the slope drops below 60 % and 30 % of $\bar{s}_M$, respectively (red dot and blue square in Fig. 3B). We defined $\bar{s}_M$ as the field mound slope s_M averaged over all the surveyed mounds. The slope s_M was computed from the elevation of the surveyed mound and platform plots. $\bar{s}_M$ and s_M are shown for reference in Fig. 3B.

For each mound candidate, we then identified the following predictors: (i) the elevation of the mound edge and base (z_e and z_b, respectively), from the elevation radial distribution; (ii) the elevation of the mound center, z_c; (iii) the height of the mussel mounds (H_M), by subtracting z_b from z_c; (iv) the radius of the mussel mound (R_M in Fig. 3B), as the distance between the center and the base of the mound; (v) the average slope of the mound side (s_L in Fig. 3B), as the ratio between the height of the mound side ($H_S = z_e - z_b$) and the planimetric distance between the mound edge and base (R_S in Fig. 3B). (vi) the skewnesses (G_p) of the elevation, slope, and curvature distributions (corresponding to the subscripts $p = z, s, c$, respectively), which were calculated as:

$$G_p = \frac{\frac{1}{N}\sum_a (p-\bar{p})^3}{\left(\frac{1}{N}\sum_a (p-\bar{p})^2\right)^{3/2}}, \quad (1)$$

where $\bar{p}$ is the mean value of the considered variable, p is its value in the a^{th} annulus and N is the total number of annuluses.

The predictors, except for the skewness, are visually reported in Fig. 3B. All the predictors are listed in Table 1.

2.4. Random Forest classifier (STEP 4)

To determine the spatial distribution of the mussel mounds, we used a Random Forest classifier. A Random Forest consists of many individual decision trees operating as an ensemble. Given a dataset of elements to classify, each tree gives a class prediction to each element by using some predictors. For each element, the class with the higher number of votes becomes the prediction of the Random Forest model. In our case, the dataset consisted of the candidate mounds identified in STEP 2 (i.e., Section 2.3.2), the predictors were the ones described in STEP 3 (i.e., Section 2.3.3), and the classes were two: mound and not-mound. The classification procedure was repeated for each of the MinE and AveE rasters we identified in STEP 1 (Section 2.3.1).

We trained and tested the Random Forest classifier using a dataset of 150 locations on the marsh system. Among these locations, 42 were surveyed on the highest point of the mussel mounds, 39 were the surveyed marsh platform areas adjacent to them, where no mounds are present, 38 were surveyed close to a creek, where no mounds are present, and 31 were points located on the marsh levees and edges, which are not located on mussel mounds. Our cross-validation and test datasets contained 120 and 30 entries, which correspond to 80 % and 20 % of the dataset, respectively. We used the first database to perform a k-fold cross-validation, with k equal to 4 (i.e., each fold contains 30 entries). We then used the test

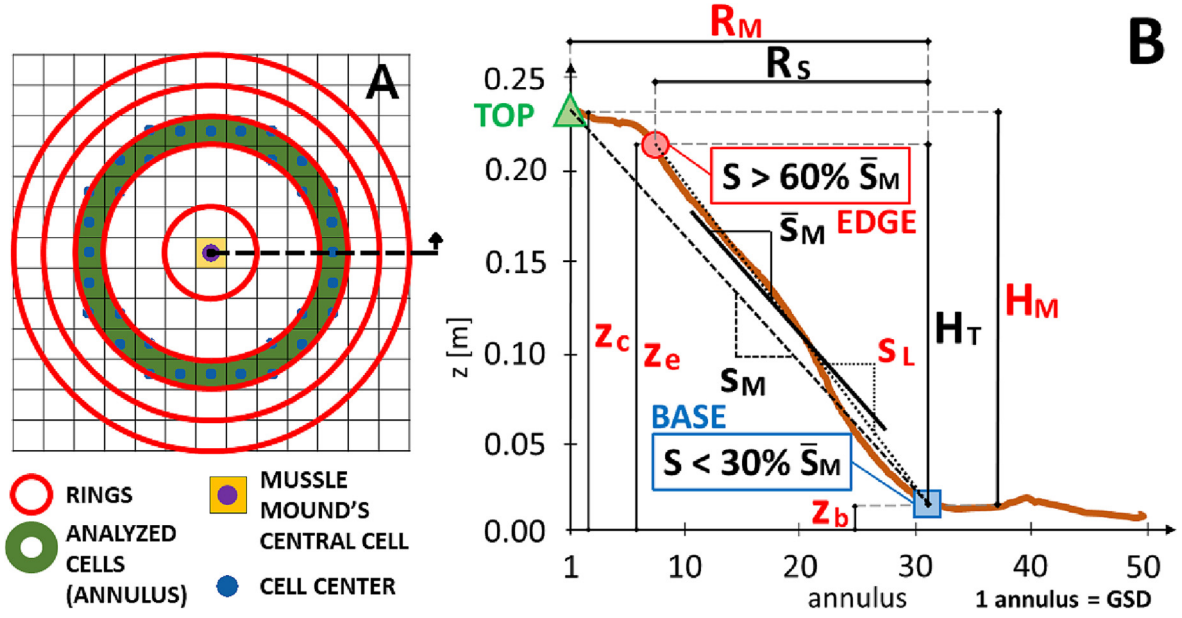

Fig. 3. (A) Planar description of the method used to determine the distribution of the average elevation, slope, and curvature in the neighborhood of the cells containing the candidate mounds (central orange cell). Consecutive rings (red circles) form an annulus (green band) containing the cells whose centers (blue dots) are used to determine the average of the considered parameter. (B) Visual description of the predictors (in red) obtained from the elevation layers based on the UAV-Lidar point cloud, for all the candidate mounds. The red and blue markers identify the edge, and base of the mussel mounds, and are computed from the distribution of the average elevation in the area surrounding the marsh center (light brown line). The green marker identifies the center of the mussel mound.

Table 1
List of the predictors used by the Random Forest classifier. U.M. stands for unit of measurement.

Description	Name	U.M.
Skewness of the average elevation	G_z	–
Skewness of the average slope	G_s	–
Skewness of the average curvature	G_c	–
Slope of the mussel mound side	s_L	–
Mussel mound edge elevation	z_e	m
Mussel mound base elevation	z_b	m
Mussel mound center elevation	z_c	m
Mussel mound height	H_M	m
Mussel mound radius	R_M	m

dataset to evaluate the performances of the cross-validated classifier. We finally used the tested Random Forest to classify the candidate mounds identified in STEP 2, using the predictors obtained in STEP 3. The model results were the position of the mussel mounds in the study area. Once the model was tested, we trained it again, using the entire dataset (150 entries), and we used this newly trained model to identify the mussel mounds in the study domain.

2.4.1. Accuracy analysis

To determine which combination of predictors maximizes the correct identification of the mussel mounds, we performed an accuracy analysis. For this analysis, we used the validation and test datasets as the ground-truth dataset. We performed a distinct accuracy analysis for the MinE and AveE rasters.

For each point, the ground-truth class was compared to the class assigned by the Random Forest classifier, and a confusion matrix was generated to determine the model accuracy. Confusion matrixes are used in machine learning and data analysis to understand which portion of the classified data is correctly classified, from a comparison with the reference (i.e., ground-truth) data (Story and Congalton, 1986). Reference and classified data occupy the column and rows of the matrix. The number of rows and columns corresponds to the number of the classes (in our case two: "mussel mound" and "no mussel mound"). The diagonal of the matrix indicates the correctly classified data per class, and so the agreement between reference and classified datasets. The remaining cells indicate the misclassified data. An additional row and column contain the total number of classified and reference data per class, respectively. Using these values, we calculated the following accuracy metrics of the classifier. The "overall accuracy" (OA), he "producer's accuracy" (PA), the "user's accuracy" (UA) and the kappa (κ) value (see Supplementary Material, Section S2.5). The latter ranges from -1 to $+1$. The value 0 represents the agreement obtained from a random classifier, while $+1$ and -1 represent perfect agreement and disagreement between the results obtained from the two classifiers, respectively (Cohen, 1960). We interpreted the κ value as follows: ≤ 0.00 indicates no agreement; ≤ 0.20 indicates none to a slight agreement, ≤ 0.40 indicates fair agreement, ≤ 0.60 indicates moderate agreement, ≤ 0.80 indicates substantial agreement; ≤ 1.00 indicates almost perfect agreement (Cohen, 1960). We extended this interpretation to OA, PA, and UA.

The accuracy analysis was performed by using the predictors we calculated in STEP 3. In the following, we report the results for the classification performed by using the predictors singularly, all together, and for the combinations that give the best results.

2.5. Geometric properties of mussel mounds

We developed a MATLAB algorithm to calculate the volume and the surface of the mussel mounds. The algorithm was applied to both the surveyed mussel mounds and the ones obtained from the Random Forest classifier. The algorithm took as input a raster dataset and the location of a classified mound and identified its volume and area as follows: (i) in a 21 cells $\times$ 21 cells stencil centered on the center of the mound, the algorithm defined as mounds the cells that had an elevation greater or equal than the mound base and a distance from the center of the mound smaller than or equal to its radius R_M. (ii) A dilation-erosion filter (see Supplementary Material, Section S3) was applied to remove isolated cells that did not belong to the mound. (iii) The mound planar area was calculated by summing the areas of the mound cells. (iv) The height of the mound cells was defined as the difference between the elevation of the mound cell and the mound base. (v) The volume of each mound cell was computed by multiplying its height by its area. By summing these volumes, the algorithm computed the mound volume.

3. Results

3.1. Accuracy analysis results

3.1.1. Cross-validation phase

In this section, we describe the results of the cross-validation we performed for the Random Forest classifier applied to the MinE and AveE rasters.

The results reported in Table 2 indicate that both for the MinE and AveE rasters, the classifier accuracy (i.e., the capability to correctly classify the mound candidates) increased when more predictors were used in the classification procedure. However, also the single predictors (first nine rows) show good values of the accuracy metrics. When the classifier used one predictor and the AveE rasters, OA ranged between 0.62 and 0.83, PA ranged between 0.37 and 0.69, UA ranged between 0.54 and 0.85, and κ ranged between 0.11 and 0.63. When the classifier used one predictor and the MinE rasters instead, OA ranged between 0.56 and 0.80, PA ranged between 0.41 and 0.63, UA ranged between 0.67 and 0.84, and κ ranged between 0.16 and 0.56.

In particular, the value of κ indicates that there is a slight to moderate agreement between the classified and the reference data both for the AveE and the MinE rasters.

The best value of the accuracy metrics was observed when the classifier used as a single predictor the elevation of the mound center (z_c, seventh row). For this predictor, the value of the accuracy metrics indicated that there was a substantial agreement (κ<0.80) between the classified and the reference data for the AveE rasters, and a moderate agreement (κ<0.60) for the MinE rasters.

For the MinE rasters, we obtained the best values of all the accuracy metrics by using the three skewness G_z, G_s, and G_c (tenth row) in the RF. Using these predictors, we obtained an OA of 0.92, a PA of 0.86, a UA of 0.88, and a κ of 0.80 (substantial agreement). For the AveE rasters instead, we obtained the best values of all the accuracy metrics by using all the predictors (coupling $G_z, G_s, G_c, s_L, z_e, z_b, z_c, H_M,$ and R_M, last row) in the RF. Using these predictors, we obtained an OA of 0.94, a PA of 0.91, a UA of 0.92, and a κ of 0.87 (almost perfect agreement). These values correspond to the highest observed for the cross-validation.

These results indicate that when more than a predictor was used in the Random Forest procedure, the predictors based on the AveE rasters produce more accurate results than the ones based on the MinE rasters.

Table 2
The table contains the results of the cross-validation performed for the Random Forest classifier. The table contains the results obtained by using the predictors obtained at STEP 3 (Section 2.3.3) singularly, all together, and for the combinations that give the best results. The results are reported for both the AveE and MinE rasters. The underlined value is the best among those obtained using the AveE and MinE rasters. The bold values are the maximum observed for the considered combination of predictors used.

Classification predictors	Overall Accuracy (OA)		Producer's Accuracy (PA)		User's Accuracy (UA)		Kappa (κ)	
	AveE	MinE	AveE	MinE	AveE	MinE	AveE	MinE
Skewness elevation (G_z)	0.74	0.70	0.58	0.52	0.84	0.79	0.49	0.39
Skewness slope (G_s)	0.66	0.67	0.46	0.47	0.65	0.73	0.27	0.32
Skewness curvature (G_c)	0.57	0.62	0.37	0.45	0.54	0.71	0.11	0.26
Slope mound side (s_L)	0.62	0.56	0.42	0.41	0.59	0.59	0.20	0.16
Elevation edge (z_e)	0.75	0.78	0.57	0.61	0.75	0.75	0.45	0.51
Elevation base (z_b)	0.78	0.72	0.62	0.52	0.83	0.84	0.53	0.42
Elevation center (z_c)	0.83	0.80	0.69	0.63	0.85	0.84	0.63	0.56
Mound height (H_M)	0.73	0.65	0.56	0.47	0.82	0.67	0.46	0.28
Mound radius (R_M)	0.79	0.73	0.65	0.57	0.75	0.68	0.53	0.41
G_z, G_s, G_c	0.93	**0.92**	0.89	**0.86**	0.89	**0.88**	0.83	**0.80**
$s_L, z_e, z_b, z_c, H_M, R_M$	0.82	0.82	0.65	0.69	0.88	0.78	0.60	0.58
$G_z, G_s, G_c, s_L, z_e, z_b, z_c, H_M, R_M$	**0.94**	0.90	**0.91**	0.84	**0.92**	0.86	**0.87**	0.76

3.1.2. Test phase

The results obtained for the test phase of the accuracy analysis (Table 3) indicate that the predictors based on the AveE rasters produce similar or more accurate results than the ones based on the MinE rasters. For this reason, we report only the results related to the AveE rasters.

The results reported in Table 3 show that the classification accuracy increased when more predictors are used in the classification procedure. However, excellent results of the user's accuracy (UA) were obtained also when the classifier used only one predictor (first nine rows). In this case, the results indicate that 60 to 100 % of the mound candidates were correctly classified. The values observed for the OA (first column) and the PA (second column) range between 0.27 and 0.80, indicating fair to substantial agreement between the classified and reference data. The best performances were observed for the elevation of the mound center (z_c, seventh row), which present OA equal to 0.80, a PA equal to 0.45, and a UA equal to 1.00. Finally, the value of κ (last column) confirms the adequate classification skills obtained by using this predictor. In fact, z_c has the highest value of κ, which is equal to 0.51.

We obtained the best classification skills by using the three skewnesses G_z, G_s, and G_c (fourteenth row), which gives an OA of 0.97, a PA of 0.83, and a UA of 1.00. These values indicate that >80 % of the mound candidates are correctly classified. The quality of the results is underlined by the large value reached by κ (0.89). The statistical parameters we obtained by coupling s_L, z_e, z_b, z_c, H_M, and R_M (penultimate row) are lower than those obtained by using the three skewnesses. Finally, the results we obtained by using all the calculated predictors in the classification procedure (last row) are similar to those observed by using the three skewnesses. For this reason, we decided to use all the predictors in the classification process.

3.2. Mussel mound distribution in the marsh system

The map in Fig. 4A shows the mussel mounds distribution (blue dots) we obtained in our marsh system by using our classification algorithm on the AveE rasters. Fig. 4B, C, and D show the three locations where we surveyed the mussel mounds (cyan circles). A comparison between the location of the cyan circles and blue dots indicates that 95 % of the surveyed mounds were identified by the classifier. Among these, only a few mussel mounds were identified in the highly vegetated creek levees and marsh edges (Fig. 4A).

The map in Fig. 4A also shows that mussel mounds are preferentially located close to the creek heads, where the hydroperiod is longer and nutrient availability is higher (Wiegert et al., 1983). The map also shows that mounds density declines approaching the marsh edge and the lower marsh, where nutrient delivery is lower, and predation intensifies. Moreover, we note that mussel mounds are almost absent between survey locations B and C, and in the southeastern portion of location B. The particularly low elevation of these areas may cause excessive saltwater stagnation in them, which hinders mussel settlement and growth (Leonard et al., 1998; Alfaro, 2005). In addition, approximately 200,000 mussels were transplanted from location C into this location from location B by Crotty et al. (2023).

To summarize, our classification algorithm successfully identified 8010 mussel mounds on the marsh platform, resulting in a density of approximately 0.08 mounds per square meter. To estimate the corresponding mussel density, we conducted a visual inspection of 39 mounds within the study area, which contained an average of around 134 mussels each, with a range of 8 to 304 individuals per mound. These findings are consistent with

Table 3
The table contains the results of the test performed for the Random Forest classifier. The table contains the results obtained by using the predictors obtained at STEP 3 (Section 2.3.3) singularly, all together, and for the combinations that give the best results. The results are reported for both the AveE and MinE rasters. The underlined value is the best among those obtained using the AveE and MinE rasters. The bold values are the maximum observed for the considered combination of predictors used.

Classification predictors	Overall Accuracy (OA)		Producer's Accuracy (PA)		User's Accuracy (UA)		Kappa (κ)	
	AveE	MinE	AveE	MinE	AveE	MinE	AveE	MinE
Skewness elevation (G_z)	0.67	0.60	0.31	0.29	0.80	1.00	0.27	0.27
Skewness slope (G_s)	0.70	0.73	0.36	0.36	1.00	0.80	0.37	0.35
Skewness curvature (G_c)	0.67	0.47	0.27	0.18	0.60	0.60	0.19	0.02
Slope mound side (s_L)	0.77	0.70	0.42	0.25	1.00	0.40	0.46	0.13
Elevation edge (z_e)	0.77	0.73	0.42	0.38	1.00	1.00	0.46	0.41
Elevation base (z_b)	0.70	0.67	0.36	0.31	1.00	0.80	0.37	0.27
Elevation center (z_c)	0.80	0.70	0.45	0.36	1.00	1.00	0.51	0.37
Mound height (H_M)	0.77	0.83	0.42	0.50	1.00	1.00	0.46	0.57
Mound radius (R_M)	0.73	0.80	0.36	0.44	0.80	0.80	0.35	0.45
G_z, G_s, G_c	**0.97**	0.93	**0.83**	0.71	**1.00**	**1.00**	**0.89**	0.79
$s_L, z_e, z_b, z_c, H_M, R_M$	0.90	0.83	0.63	0.50	**1.00**	**1.00**	0.71	0.57
$G_z, G_s, G_c, s_L, z_e, z_b, z_c, H_M, R_M$	0.93	**0.95**	0.71	**0.83**	**1.00**	**1.00**	0.82	**0.89**

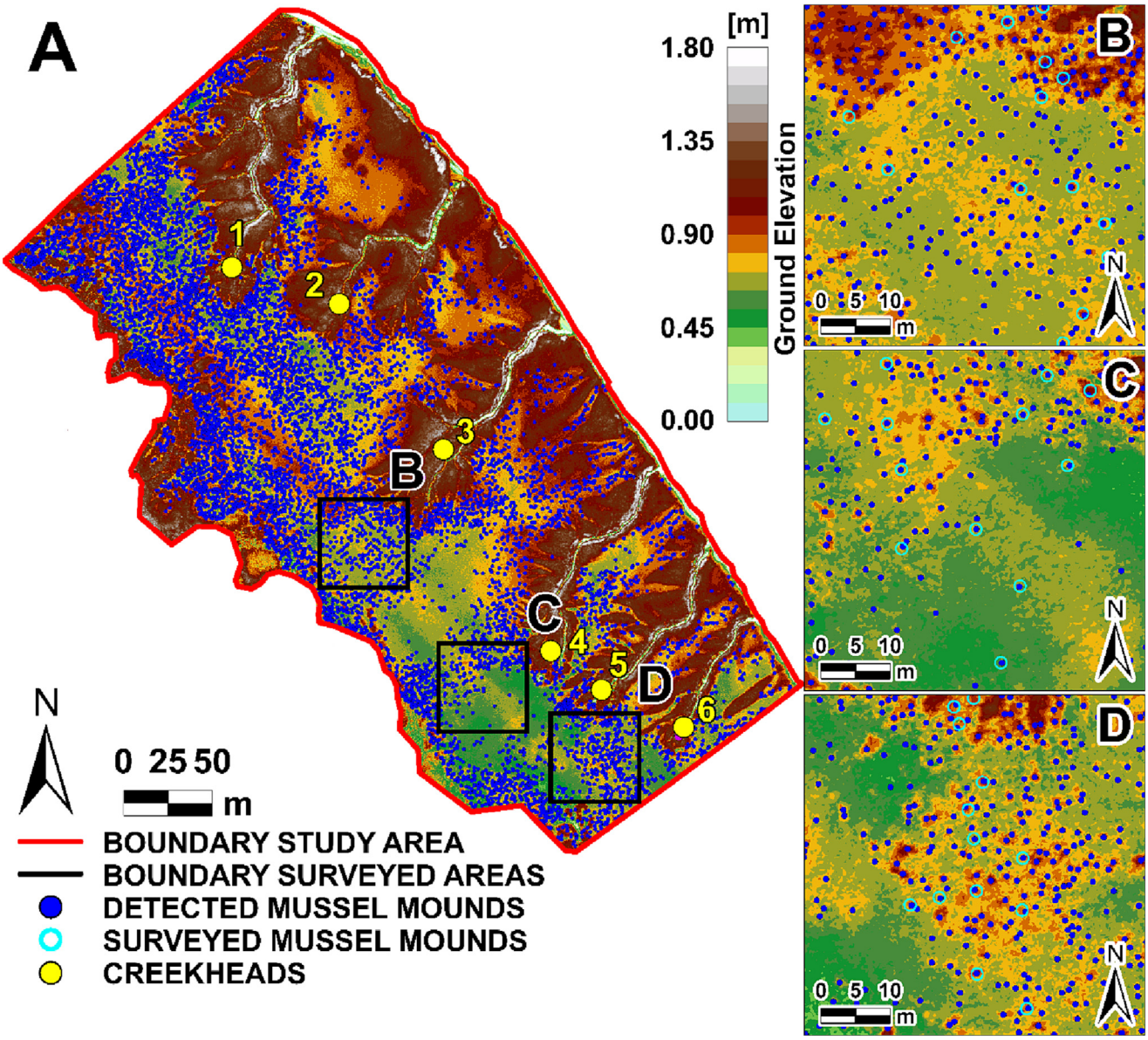

Fig. 4. Spatial distribution of the mussel mounds (blue dots) identified in the marsh system (A) by applying our classification algorithm to the AveE rasters, and at the three survey locations (insets B, C, D) we considered in our marsh system. The numbered yellow dots in (A) indicate the location of the six creek heads. The cyan circles in the insets indicate the mussel mounds we surveyed at the three locations.

previous research conducted in similar wetlands (Kuenzler, 1961; Smith and Frey, 1985; Angelini et al., 2016; Derksen-Hooijberg et al., 2018a). Therefore, we can conclude that our study area has an estimated mussel density of around 10.7 individuals per square meter, which aligns with the results of prior studies that have conducted comprehensive surveys of mussel density and coverage in marshes within this region (Angelini et al., 2016; Crotty and Angelini, 2020; Crotty et al., 2020).

3.3. Distribution of mussel mound characteristics

In this study, we divided mussel mounds into three groups: small, medium, and large. Small mussel mounds have $H_M \leq 0.05$ m and $R_M \leq 0.30$ m. Medium mussel mounds have $H_M \leq 0.15$ m and $R_M \leq 0.60$ m. Large mussel mounds have $H_M \geq 0.15$ m and $R_M \geq 0.60$ m.

The maps in Fig. 5A and C show the spatial distribution of the height (H_M) and the radius (R_M) for the mussel mounds we identified in the study domain.

From these maps, we note that small mussel mounds ($H_M \leq 0.05$ m - $R_M \leq 0.30$ m) more commonly occur on the marsh platform close to the marsh edge, the middle part of the marsh platform, where elevation is lower, and the southern part of the domain. In these areas, the low water fluxes, nutrient loads, and oxygen inputs may limit the transport and survival of mussel larvae, their deposition, and for those that settle, their growth (Leonard et al., 1998; Alfaro, 2005). Because of their large distance from the creek heads, nutrient and oxygen inputs are low close to the marsh edge and in the middle part of the platform. At the southern part of the domain, instead, the small cross-section and small length of the adjacent tidal creeks likely limit water fluxes and thus nutrient and oxygen exchanges.

Fig. 5A and C also show that the large mounds ($H_M \geq 0.15$ m - $R_M \geq 0.60$ m), occupy the northern part of the domain. Here mussel mounds occupy the heads of the two biggest tidal creeks in the salt marsh system (i.e., the first two from the northern boundary), where nutrient loads are high (Kuenzler, 1961; Stiven and Gardner, 1992; Angelini et al., 2016).

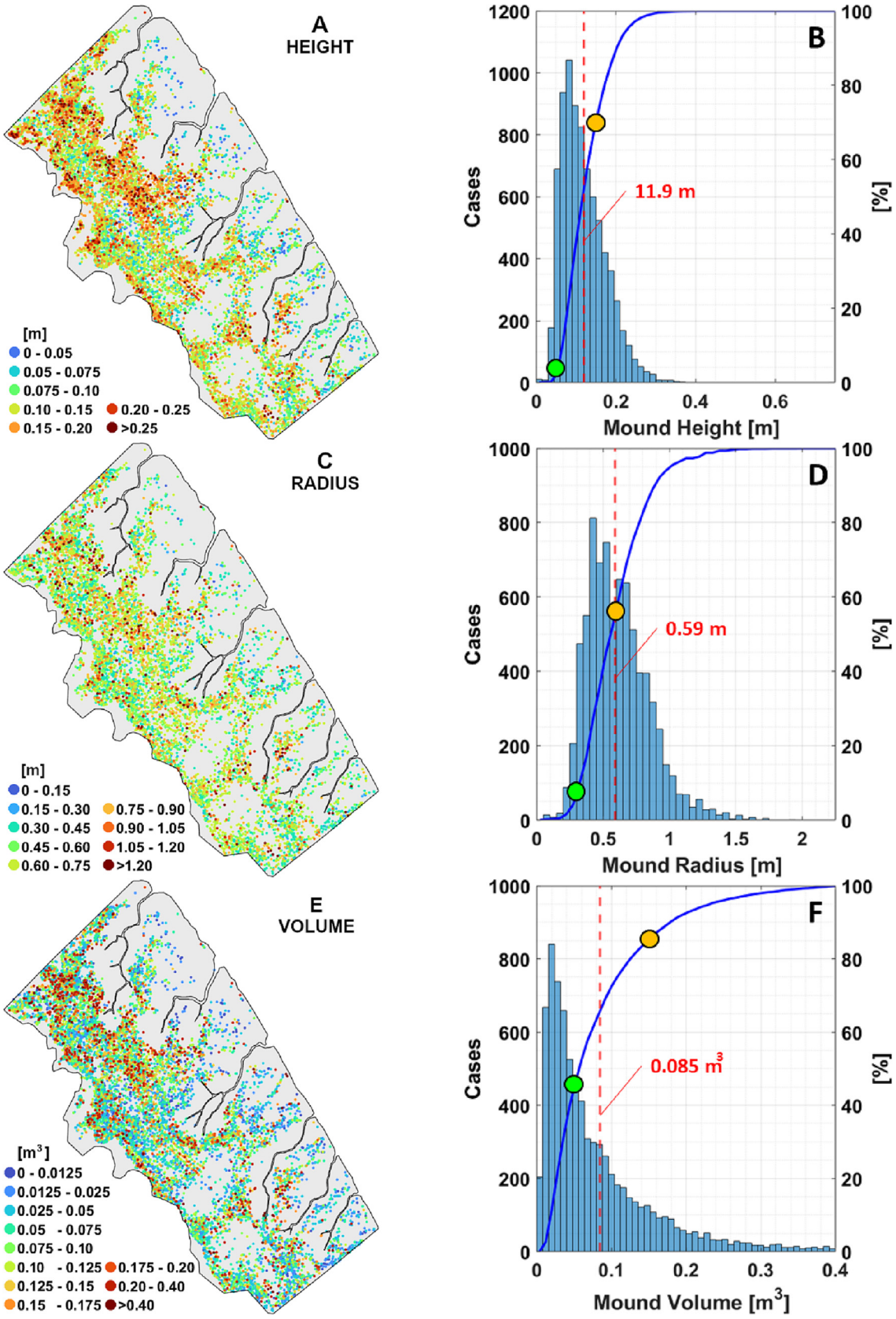

Fig. 5. Spatial (maps on the left figures), partial (blue bins on the right figures), and cumulative (continuous blue line on the right figures) of: (A-B) the height, (C-D) the average radius, and (E-F) the volume, of the mussel mounds we identified in the model domain. The green dots indicate the percentage of mussel mounds at the threshold between small and medium-size mounds. The orange dots indicate the percentage of mussel mounds at the threshold between medium-size and large mounds.

Among these large mounds, the ones with $R_M \geq 1.00$ m, represent agglomerations of different mussel mounds and are the closest to the creek heads.

Finally, the maps in Fig. 5A and C show that medium-sized mussel mounds ($H_M \leq 0.15$ m - $R_M \leq 0.60$ m) are spread all over the salt marsh system. They coexist with the small mussel mounds, except at the marsh edge, where medium-sized mounds are absent. They also coexist with large mussel mounds at the creek heads.

Fig. 5B and D show the probability (blue bars) and cumulative (continuous blue line) distributions of H_M and R_M for the mussel mounds we identified in the study domain. The distributions are defined by using 71 and 45 classes, at intervals of 2.5 cm and 5 cm, respectively. Both the parameters show a positively skewed (i.e., skewed to the right) distribution. For each distribution, the vertical dashed line indicates its mean value, which is equal to ~12 cm for the mound height, and 59 cm for the mound radius. Both of them are in the range of literature values (Smith and Frey, 1985). In Fig. 5B and D, the green and orange dots on the cumulative distributions indicate the upper thresholds for small, medium, and large mounds. Considering the mound height, small, medium, and large mounds are ~5 %, ~65 %, and ~35 % of the classified mounds, respectively. Considering the mound radius, they are ~10 %, ~45 %, and ~45 % of the classified mounds, respectively.

The map in Fig. 5E shows the spatial distribution of the volume (V_M) of the mussel mounds we identified in the study domain. As we observed for the height and the radius, while the small ($V_M \leq 0.05$ m^3) and medium ($V_M \leq 0.15$ m^3) mounds preferentially occupy the marsh edge, and the ponded marsh, the large mounds ($V_M \geq 0.15$ m^3) grow close to the creek heads.

As reported in Fig. 5F, the volume presents a positively skewed distribution, where most of the mounds have a small-medium volume. Both the probability and cumulative distributions were obtained by dividing the volume dataset into 50 classes, which range is 0.008 m^3. The green dot in Fig. 5F shows that large mounds are ~15 % of the total. The orange dot indicates that the small mounds are ~45 % of the total mounds. Consequently, medium mounds are ~40 % of the total. Finally, the average mound volume is equal to ~0.085 m^3, due to the high number of small mounds.

Overall, the results in this section show that the distribution of mussel mound height, radius, and volume, strongly depends on their distance from the creek heads, which is the main marsh access point for nutrients and oxygen (Kuenzler, 1961; Stiven and Gardner, 1992; Angelini et al., 2016).

Fig. 6A and B show the distribution of the average mussel mound height and radius at progressive distances (5 m resolution) from the head of the six creeks in our salt marsh (yellow dots in Fig. 4). The values are computed using the spatial distributions obtained from the Random Forest classifier. The results reported in Fig. 6 confirm that tall and large mussel mounds develop close to the creek heads, except for the second creek (i.e., the second from the northern boundary of the study area). For this creek, both mussel mound height and radius increase until they reach a maximum of ~50 m from the creek head, and then decrease. Finally, because high and large mussel mounds grow close to the creek placed at the western boundary of the study area, both mound height and radius increase >50 m from creek heads 1 and 5.

The map in Fig. 7A shows the spatial distribution of the distances between the mussel mounds detected in the study domain. The distances were calculated by using the TIN (Triangular Irregular Network) generation tool (i.e., "*Create TIN*") in ArcGIS. The TIN satisfies the Delaunay triangle criterion, which ensures that no vertex (i.e., the location of the classified mussel mounds) lies inside any of the circumcircles of the triangles in the network. The Delaunay criterion maximizes the minimum angle of all the triangles in the TIN, to avoid long and thin triangles. Fig. 7A indicates that the distance between mounds is lower close to the creek heads, where values range between 0.75 m and 2.50 m, and increase to values higher than 8 m at the marsh edges. Fig. 7B underlines that the minimum distance between mounds is ~0.75 m and that the average distance is 3.20 m. Note that distances follow a distribution with a long tile toward high values.

3.4. Mussel mound geometrical properties

In this section, we discuss the relationships between the geometric properties of the mussel mounds we identified in our study area. Fig. 8A shows the good linear relationship (Table 4, first row) between the height and the radius of mussel mounds (R^2 ~ 0.53). However, because of its high slope (i.e., 4.684), this relationship indicates that mussel mounds grow more laterally than vertically. Fig. 8B shows a strong correlation between the volume and the radius of the mussel mounds (R^2 ~ 0.80). The relationship is non-linear (Table 4, third row). Fig. 8C shows a good relationship between the volume and the height of the mussel mounds (R^2 ~ 0.62). As we observed for the radius, the relationship is not linear (Table 4, third row), and is not well defined for a mound radius larger than ~0.30 m. These results indicate that, over a certain threshold height, the volume of the mussel mounds increases because of their lateral expansion, as reported in Fig. 8D, which shows the relationship between the volume and the mussel mound height and radius (Table 4, last row).

4. Discussion

Here, we developed a new algorithm that estimates the spatial distribution and the dimension (i.e., height, radius, and volume) of the mussel mounds in a densely vegetated salt marsh, by using a Random Forest classifier. The results indicate that the distribution and properties of the mussel mounds strongly depend on their distance from the tidal creeks and the marsh edge. This suggests that the properties of the tidal network, and in particular, the distribution and the dimensions (both longitudinal and cross-sectional) of the creeks, influence the settling and growth of mussel mounds in a salt-marsh system.

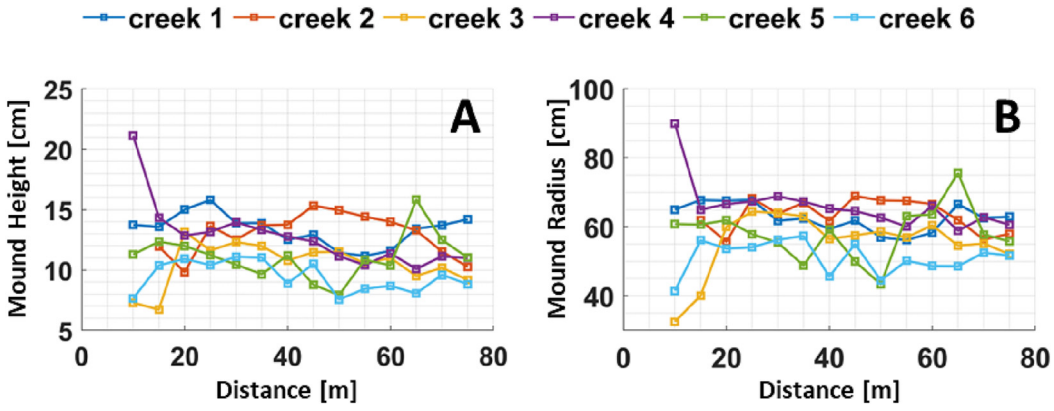

Fig. 6. The distribution of the average mussel mound height (A) and radius (B) at progressive distances (*x*-axis) from the head of the six creeks in our study area. The values are computed from the spatial distributions obtained from the Random Forest classifier. The creek head locations used for the computation are the yellow dots in Fig. 4.

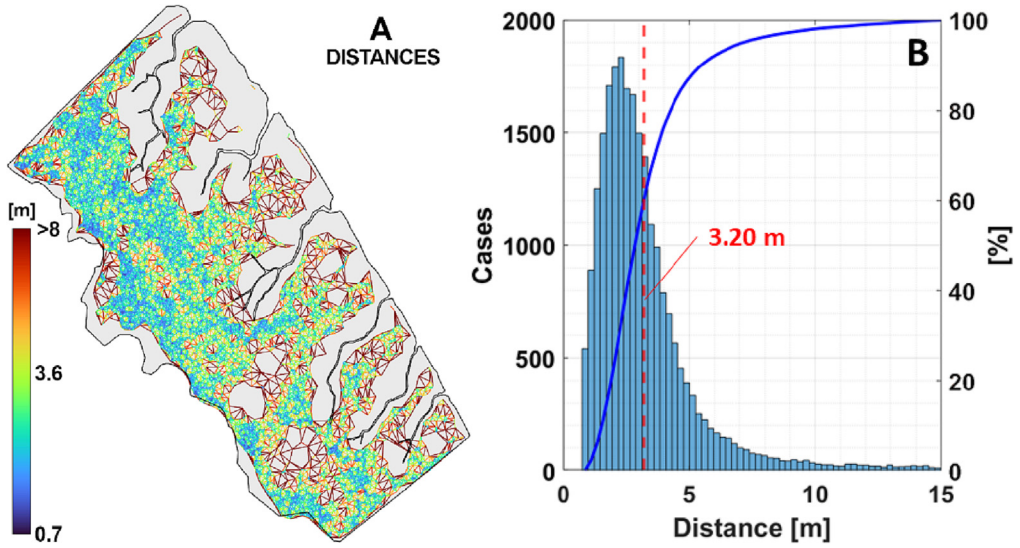

Fig. 7. The spatial distribution (A) and the probability and cumulative distributions (B) of the distances between the mussel mounds identified in the study area.

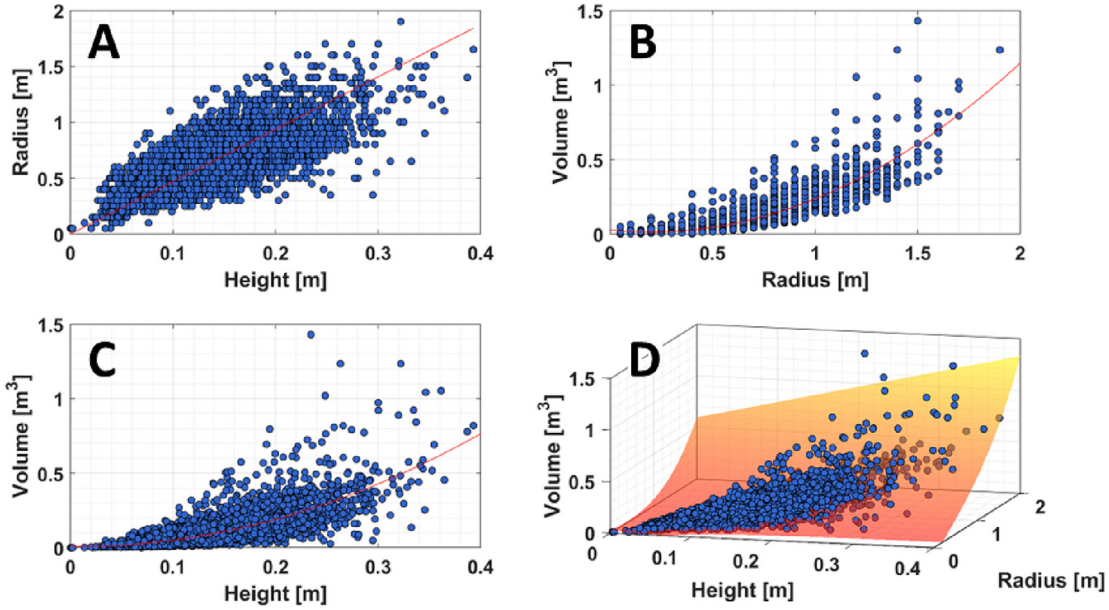

Fig. 8. The graphs show the relationships between: (A) mounds height and radius; (B) mounds volume and radius; (C) mounds volume and height; (D) mounds height, radius, and volume. The blue dots are the values observed for the detected mounds. The red lines and surface represent the regression between the considered variables.

4.1. Mussel mounds distribution

Our algorithm estimates that ~8000 mussel mounds populate our salt marsh. This value corresponds to a density of ~10.7 mussels m^{-2}, which is in the lower range of the values observed in other salt marshes in Georgia (Kuenzler, 1961; Jordan and Valiela, 1982; Smith and Frey, 1985; Kneib and Weeks, 1990).

The low mussel density may be related to the flooding time (the hydroperiod) of our study area. Our domain is flooded for ~4.5 h day^{-1} (see Supplementary Material, Section S4), which is lower than the values associated with marshes with higher mussel densities (Kuenzler, 1961; Smith and Frey, 1985; Kneib and Weeks, 1990). A low hydroperiod hinders mussels settling, growth, and survival, because, as filter feeders, they preferentially occupy areas with high flows where food and oxygen availability are large (Leonard et al., 1998; Alfaro, 2005). In addition, the density could be

Table 4
Relationship between mound height (H_M), radius (R_M), and volume (V_M) we observed for the mounds we detected in our study area, and the value of the R^2.

x	y	z	Relationship	R^2
H_M	R_M	–	$y = 4.684x$	0.53
R_M	V_M	–	$y = 0.029 - 0.145x + 0.352x^2$	0.80
H_M	V_M	–	$y = 0.008 - 0.059x + 4.87x^2$	0.62
H_M	R_M	V_M	$z = 0.023 - 0.303x - 0.043y + 1.290xy + 0.002y^2 - 0.109xy^2 + 0.081y^3$	0.84

slightly underestimated due to the lower penetration of Lidar pulses in the tall *Spartina alterniflora* that covers them. Considering that ~15 % of mussels populating a marsh system are contained in areas with tall *Spartina alterniflora* (Kuenzler, 1961), we estimate that mussel density in our study domain is equal to ~3.3 mussels m^{-2}.

Our results indicate that mussel mounds occupy a surface of ~9820 m^2, which is ~14 % of the low vegetated salt marsh area (i.e., 0.07 km^2) and ~10 % of the entire domain (i.e., 0.1 km^2). To calculate the low vegetated area, we subtracted the Digital Elevation Model from the Digital Surface Model obtained from the UAV-Lidar point cloud collected in the domain, and we sum the surface of the cells in which the difference was lower than 0.65 m. The percentage of marsh surface coverage obtained by our algorithm (i.e., ~10 %) is higher than those observed in other studies performed close to our marsh system (i.e., 1–7 %; Kuenzler, 1961; Crotty and Angelini, 2020). Crotty et al. (2023) observed that mussel mounds increase the vertical accretion of the salt marsh and that this increase is proportional to the area they occupy in the platform. Therefore, our results suggest that this marsh has a higher potential to keep up with the sea level rise than the ones considered in the studies cited above. In addition, vegetation growth, survival, and recovery are enhanced above mussel mounds (Angelini et al., 2016; Derksen-Hooijberg et al., 2018b). Therefore, our results indicate that, compared to other systems, our marsh has a higher resilience to climatic extremes, such as drought, and consequently a lower probability of degradation in the short and long term.

The mounds identified in our marsh have a total volume of ~680 m^3, which corresponds to an average addition of ~7 mm to the marsh elevation. Recently, numerical and field analyses have been performed by our team (Crotty et al., 2023), to quantify the contribution of mussels to salt marsh accretion in the same location. Results indicate that mussel mounds increase marsh aggradation by about 4 mm $year^{-1}$, which corresponds to a volume of 400 $m^3 year^{-1}$. Considering that the volume of our mounds is ~680 m^3, the results from Crotty et al. (2023) suggest that their growth can occur in about 1.7 years. This result confirms the important contribution of ecosystem engineers to marsh aggradation and resilience to sea-level rise, highlighted in this paper, and underlines the importance of investigating the efficacy of restoration projects using mussel mounds.

The height of the mussel mounds is not negligible compared to the water depth on the marsh platform (i.e., ~15 cm vs. 40–80 cm along the southeast of the US). Therefore, mussel mounds markedly influence the hydrodynamics of the marsh platform. The presence of mussel mounds, and the increase in vegetation density and height above them (Angelini et al., 2016), enhances marsh roughness and consequently reduces the average velocities over the marsh system. Lower velocities facilitate mussel larvae settlement and sediment deposition, promoting mound growth and marsh aggradation. Moreover, high mounds and denser vegetation patches divert water fluxes to less vegetated regions of the marsh (Pinton et al., 2020a), enhancing the transport of larvae, nutrients, sediments, and oxygen in these areas, consequently favoring the growth of new mounds. In the long term, this may increase the number of mussel mounds in the marsh, consequently improving the capability of the marsh system to keep up with the rising sea level.

The results in Fig. 7 indicate that the distance between adjacent mussel mounds has a lower limit, which corresponds to ~0.75 m. This suggests that mussel mounds have an influence area, where the growth of new mounds is discouraged. These results consequently suggest that only a limited number of mounds can grow in a salt marsh, so mounds density could have a higher limit. The existence of a maximum density of mussel mounds in the marsh system indicates the presence of a maximum contribution of mussel mounds on the vertical accretion of the marsh since Crotty et al. (2023) indicate that mussel mounds increase the vertical accretion proportionally to the area they occupy in the platform. The distribution in Fig. 7B underlines the presence of a mode distance between mussel mounds, which corresponds to ~2.00 m. By monitoring the mussel mounds over time, we would be able to understand whether the system has reached a max mound density or if that can further increase.

4.2. Mussel mound geometrical properties

The presence of the threshold height for the mussel mounds reported in Section 3.4, is commonly observed in bivalve aggregations (Ridge et al., 2015; Crotty and Angelini, 2020; Bost et al., 2021). Crotty and Angelini (2020) identified an optimal elevation, or "ceiling", as the maximum elevation reached by the mussel mounds in the marsh system. We then analyzed the distribution of the mussel mound height and elevation, with respect to the surrounding marsh platform elevation, along two transects located in the creek head area in from of the two northern creeks in the study domain (cyan lines in Fig. 9). The results indicate that, for the two transects, an elevation ceiling is visible and ranges between 0.70 and 0.80 m AMSL (green lines and triangles in Fig. 9), and the mussel mound height decreases (red lines and squares in Fig. 9) when the elevation of the adjacent platform increases (blue lines and dots in Fig. 9), as observed in Crotty and Angelini (2020).

4.3. Applications of the mussel mounds identification model

Information about mussel mounds distribution and geometry can be used by numerical modelers, biologists, and scientists, to evaluate the impact of these ecosystem engineers on coastal areas, as well as by local stakeholders, to regulate mussels harvesting, and take proactive decisions to enhance coastal protection.

Our algorithm can be used, in conjunction with results from numerical models and field sampling, to evaluate which hydrodynamic (i.e., water fluxes magnitude), morphology/topography (i.e., elevation distribution, sediment transport, and tidal network characteristics), and biological variables (i.e., vegetation cover, nutrients availability, as well as abundance and typology of predators) mostly influence mussel formation and growth. For instance, our results can be used to calibrate a population dynamics model for mussel mound evolution. The model could be coupled with a numerical hydrodynamic and morphodynamic model, to predict the evolution of a marsh system accounting for the effect of dynamically evolving mussel mounds.

When mussels feed, they preferentially remove suspended sediments (Moody and Kreeger, 2020), bacteria (Wright et al., 1982), and nutrients (Jordan and Valiela, 1982), from the water column, improving water quality and clarity and playing a key role in the nutrient cycle (Kreeger et al., 2011). In addition, previous studies found that mussels filter up to ~2 times the particulate nitrogen exported by the salt marsh because of tidal exchange (Jordan and Valiela, 1982). Therefore, mussels mitigate eutrophication (Kemp et al., 2005), increase marsh productivity (Angelini et al., 2015), and increase the abundance and diversity of commercial fisheries (Julien, 2018) and invertebrates (Angelini et al., 2015). For all these reasons, projects that restore nutrient balance are being studied (Will et al., 2012; Galimany et al., 2017). In this perspective, recent studies identified temperature and seston variability as the main drivers of mussels filtration services in coastal salt marshes (Moody and Kreeger, 2020). However, since the magnitude of filtration depends on mussel biomass, the estimate of mussel filtration services requires the knowledge of their abundance and spatial distribution, as well as their feeding time and nutrient availability (Moody and Kreeger, 2020). Our classifier can be used to define the location of mussel mounds in these models. Coupled numerical hydrodynamic and particle tracking models (Mandlburger et al., 2015) can be used to evaluate the contribution (filtration services) of mussel mounds in coastal and estuarine water quality. This approach can be used to track the dispersion of nitrogen over time and space, and to analyze the effect of seasonality, the mutual interaction (competition) between mussels, and the presence of downstream effects (Gray et al., 2021) on nitrogen filtration.

Finally, the mussel harvesting industry can benefit from our method. An interactive map based on our identification method can be used by local managers to set harvesting boundaries (Julien, 2018). Harvesters can be informed of the location, the dimension, and the conditions of the mussel mounds in a certain area, to avoid overharvesting. This is important considering that commercial harvesting of ribbed mussels has increased

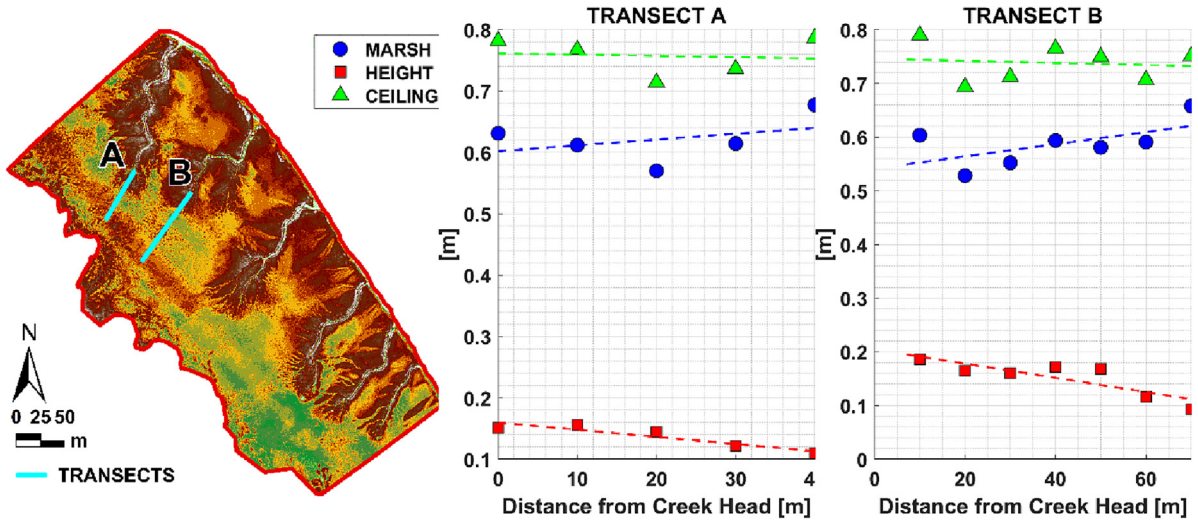

Fig. 9. Location of the two transects (cyan lines in the map on the left) where we calculated the average: (blue lines and dots) elevation of the marsh platform; (red lines and squares) height of the mussel mounds; (green lines and triangles) elevation of the mussel mound "ceiling" elevation.

substantially over the past years on the East coast (Julien, 2018). Due to the importance of mussel mounds on marsh resilience and restoration, the method proposed in this study can be used to identify marsh conservation priorities, detect areas where enhancing mussels may boost marsh resilience, and also support the design of marsh restoration projects that may attempt to mimic the marsh distribution patterns (e.g. mound densities, heights, distances between mounds) observed in natural marsh system in efforts to exploit the benefits of the mutualism.

4.4. Method advantages and limitations

Using the proposed method, the location and the geometric properties of the mussel mounds can be easily identified in the marsh platform, especially in the areas occupied by small and medium *Spartina alterniflora*. However, the identification of mussel mounds in highly vegetated areas, such as creek levees and marsh edges (Fig. 4A), is limited because (i) tall, dense vegetation occupying these features limited Lidar pulse penetration, rendering ground elevation changes difficult to identify (Cohen, 1960; Kemp et al., 2005); (ii) while vegetation is taller when growing among mussels on the marsh platform (Angelini et al., 2016), its height is more uniform on creek levees and the marsh edge, providing less, if any, indication of mussel presence. This limitation could be bypassed by operating low-altitude flights (Wang et al., 2017). This procedure allows the collection of high-density point clouds and increases the probability for laser pulses to penetrate the dense vegetation layer and reach the ground (Wang et al., 2017) and then the mussel mounds. However, during our surveys, we note that a very limited number of mussel mounds occupy the creek levees and the marsh edge in our study domain. This observation is consistent with prior observational work summarizing mussel distributions across these marshes (Kuenzler, 1961; Lin, 1989; Crotty and Angelini, 2020), and suggests the limited impact of this limitation on our results.

Field surveys require extensive trampling and then perturb the marsh ecosystem, which often takes several months to recover. Although the use of UAVs can reduce the damage caused to the marsh, the proposed method is still somewhat invasive. This is because it requires actively walking on the marsh to accomplish certain tasks such as locating a land station to calibrate the GNSS sensor on the drone, finding additional targets for correct georeferencing of the collected point cloud, and surveying mussel mounds to calibrate the classifier. The first limitation can be bypassed by positioning the land station at the marsh edge. The second limitation can be solved by operating an accurate calibration of the GNSS sensor on the drone. For the third limitation, reaching the mussel mounds during high tide using a boat or kayak is a possible solution. However, at high tide, it is difficult to collect the radius, volume, and surface, of a mound, due to the high water turbidity.

The proposed method successfully detects mussel mounds, but it is limited to small areas due to the short battery life of the UAVs, which is about 30 min. To overcome this limitation, alternative aircraft such as helicopters, ultralight aircraft, and small planes can be used. However, it is important to consider that these methods have some drawbacks. Firstly, they are less flexible compared to UAVs as they require adequate landing and take-off areas. Additionally, they can be dangerous for people as they require pilots onboard. Lastly, they are generally more expensive than UAVs due to the high cost of aircraft, pilots, fuel, and landing and take-off areas. Therefore, a cost-benefit analysis should be performed at the beginning of each project to determine which remote sensing technology is the most suitable for the job.

5. Conclusions

In this study, we present a method to determine the spatial distribution and the geometry (i.e., height, radius, surface, and volume) of mussel mounds in a coastal salt marsh, by coupling a remote-sensing technique (i.e., high-resolution UAV-Lidar) with a machine-learning classifier (i.e., Random Forest). The classifier uses as predictors the skewness of the elevation, slope, and curvature distributions in the area adjacent to the mussel mounds, the lateral slope and the radius of the mussel mounds, and the elevation of the mound edge, base, and center, which are calculated from the UAV-Lidar point cloud. The sensitivity analysis we performed underlines that the algorithm can distinguish mussel mounds from non-mussel mound locations with an accuracy (UA) of ~95 %. The analysis indicates an excellent agreement between the ground-truth data we surveyed in the study domain and the classified mounds. In addition, the algorithm is scale-invariant because, as proposed in common object identification algorithms (Lowe, 2004), it uses multi-scale rasters, which resolution depends on the dimension of the mussel mounds.

The classifier identified >8000 mussel mounds, which occupy ~10 % of the study domain. Our results indicate that mussels preferentially occupy the creek head areas, where they form dense colonies of large and tall mussel mounds, they decrease in density and dimension far from the creek heads and generally avoid the creek levee and the marsh edge. This is because nutrients and oxygen concentrations are large at the creek head, and low close to the marsh edge and in the middle part of the platform. In addition, our results underline that mussel mounds density and

dimensions are larger in the northern part of the domain because the large cross-section and length of the adjacent tidal creeks produce high nutrients and oxygen exchanges. Also, our results indicate that the volume of the mounds in our marsh is ~680 m^3, which corresponds to an addition to the average marsh elevation of ~7 mm. A parallel study we performed in this area underlines that mussel mounds increase sediment deposition by ~400 $m^3 year^{-1}$. This suggests that mound growth can occur in up to 1.7 years and underlines the importance to investigate the efficacy of restoration projects using mussel mounds. Finally, our results indicate that the minimum distance between mussel mounds is ~0.75 m, suggesting that mussel mounds have an influence area, where the growth of new mounds is discouraged.

With this study, we introduce a new remote sensing technology for surveying mussel mounds in coastal salt marshes. Our method has the potential to complement and even replace traditional methods based on field surveys. By utilizing remote sensing technology, we can obtain spatial distribution data and monitor the evolutionary trends of mussel mounds with high accuracy, short time, and low cost. The knowledge gained through our method can help formulate management and conservation strategies for salt marsh ecosystems.

Finally, we want to stress that other datasets, such as point clouds obtained from satellites, aircraft, terrestrial laser scanners, and structure from motion can be used with our classifier if the spatial resolution of these datasets is comparable with the dimension of the smallest mussel mound to identify. A comparison between the results obtained using all these datasets is the subject of future research. Finally, because of the flexibility of UAVs, and the capability of our method to be used with other point clouds, as long as their resolution is greater or similar to the resolution of the one used in this study, we believe that our method can be easily applied to large-scale areas to identify mussel mounds distribution and geometric properties, providing invaluable data for future studies related to the geomorphic evolution of marshes to sea level rise and siting marsh conservation and enhancement projects.

Funding

This research was supported by the UF Informatics Institute fellowship program.

CRediT authorship contribution statement

Daniele Pinton: Conceptualization, Data curation, Formal analysis, Investigation, Methodology, Project administration, Software, Validation, Visualization, Writing – original draft, Writing – review & editing, Funding acquisition. **Alberto Canestrelli:** Project administration, Methodology, Writing – original draft, Writing – review & editing, Funding acquisition, Resources, Supervision. **Sydney Williams:** Data curation, Writing – original draft. **Christine Angelini:** Supervision, Resources, Writing – original draft. **Benjamin Wilkinson:** Supervision, Resources, Data curation.

Data availability

The data that support the findings of this study are available from the corresponding author upon reasonable request

Declaration of competing interest

The authors declare that they have no known competing financial interests or personal relationships that could have appeared to influence the work reported in this paper.

Acknowledgements

The authors want to thank the University of Georgia Marine Institute. The research in this publication was supported by the UF Informatics Institute fellowship program.

Appendix A. Supplementary data

Supplementary data to this article can be found online at https://doi.org/10.1016/j.scitotenv.2023.163707.

References

Adolph, W., Farke, H., Lehner, S., Ehlers, M., 2018. Remote sensing intertidal flats with TerraSAR-X. A SAR perspective of the structural elements of a tidal basin for monitoring the Wadden Sea. Remote Sens. 10, 1085. https://doi.org/10.3390/rs10071085.

Alfaro, A.C., 2005. Effect of water flow and oxygen concentration on early settlement of the New Zealand green-lipped mussel, perna canaliculus. Aquaculture 246, 285–294. https://doi.org/10.1016/j.aquaculture.2005.02.049.

Ali-Sisto, D., Packalen, P., 2017. Comparison of 3D point clouds from aerial stereo images and lidar for forest change detection. Int. Arch. Photogramm. Remote. Sens. Spat. Inf. Sci. 42, 1–5. https://doi.org/10.5194/isprs-archives-XLII-3-W3-1-2017.

Angelini, C., Griffin, J.N., van de Koppel, J., Lamers, L.P.M., Smolders, A.J.P., Derksen-Hooijberg, M., van der Heide, T., Silliman, B.R., 2016. A keystone mutualism underpins resilience of a coastal ecosystem to drought. Nat. Commun. 7, 1–8. https://doi.org/10.1038/ncomms12473.

Angelini, C., Van Heide, T.Der, Griffin, J.N., Morton, J.P., Derksen-Hooijberg, M., Lamers, L.P.M., Smolders, A.J.P., Silliman, B.R., 2015. Foundation species' overlap enhances biodiversity and multifunctionality from the patch to landscape scale in southeastern united states salt marshes. Proc. R. Soc. B Biol. Sci., 282 https://doi.org/10.1098/rspb.2015.0421.

Bertness, M.D., 1984. Ribbed mussels and spartina alterniflora production in a New England salt marsh. Ecology 65, 1794–1807.

Boesch, D.F., Turner, R.E., 1984. Dependence of fishery species on salt marshes: the role of food and refuge. Estuaries 7, 460–468. https://doi.org/10.2307/1351627.

Bost, M.C., Rodriguez, A.B., Ridge, J.T., Miller, C.B., Fegley, S.R., 2021. Natural Intertidal Oyster Reef Growth Across Two Landscape Settings and Tidal Ranges, pp. 2118–2131.

Brambati, A., Carbognin, L., Quaia, T., Teatini, P., Tosi, L., 2003. The lagoon of Venice: geological setting, evolution and land subsidence. Episodes 26, 264–268. https://doi.org/10.18814/epiiugs/2003/v26i3/020.

Brockmann, C., Stelzer, K., 2008. Optical remote sensing of intertidal flats. Remote Sens. Eur. Seas., 117–128 https://doi.org/10.1007/978-1-4020-6772-3_9.

Coen, L.D., Brumbaugh, R.D., Bushek, D., Grizzle, R., Luckenbach, M.W., Posey, M.H., Powers, S.P., Tolley, S.G., 2007. Ecosystem services related to oyster restoration. Mar. Ecol. Prog. Ser. 341, 303–307. https://doi.org/10.3354/meps341303.

Cohen, J., 1960. A coefficient of agreement for nominal scales. Educ. Psychol. Meas. 20, 37–46. https://doi.org/10.1177/001316446002000104.

Crotty, S.M., Angelini, C., 2020. Geomorphology and species interactions control facilitation cascades in a salt marsh ecosystem. Curr. Biol. 30, 1562–1571. https://doi.org/10.1016/j.cub.2020.02.031 e4.

Crotty, S.M., Ortals, C., Pettengill, T.M., Shi, L., Olabarrieta, M., 2020. Sea-level Rise and the Emergence of a Keystone Grazer Alter the Geomorphic Evolution and Ecology of Southeast US Salt Marshes, p. 117 https://doi.org/10.1073/pnas.1917869117.

Crotty, S.M., Pinton, D., Canestrelli, A., Fischman, H.S., Ortals, C., Dahl, N.R., Williams, S., Bouma, T.J., Angelini, C., 2023. Faunal engineering stimulates landscape-scale accretion in southeastern US salt marshes. Nat. Commun. 14, 881. https://doi.org/10.1038/s41467-023-36444-w.

Das, Sanjib, Saikia, J., Das, Soumita, Goni, N., 2015. A comparative study of different noise filtering techniques in digital images. Int. J. Eng. Res. Gen. Sci. 3, 180–191.

Derksen-Hooijberg, M., Angelini, C., Lamers, L.P.M., Borst, A., Smolders, A., Hoogveld, J.R.H., de Paoli, H., van de Koppel, J., Silliman, B.R., van der Heide, T., 2018a. Mutualistic interactions amplify saltmarsh restoration success. J. Appl. Ecol. 55, 405–414. https://doi.org/10.1111/1365-2664.12960.

Derksen-Hooijberg, M., Angelini, C., Lamers, L.P.M., Borst, A., Smolders, A., Hoogveld, J.R.H., de Paoli, H., van de Koppel, J., Silliman, B.R., van der Heide, T., 2018b. Mutualistic interactions amplify saltmarsh restoration success. J. Appl. Ecol. 55, 405–414. https://doi.org/10.1111/1365-2664.12960.

Farris, A.S., Defne, Z., Ganju, N.K., 2019. Identifying salt marsh shorelines from remotely sensed elevation data and imagery. Remote Sens. 11, 1795. https://doi.org/10.3390/rs11151795.

Galimany, E., Wikfors, G.H., Dixon, M.S., Newell, C.R., Meseck, S.L., Henning, D., Li, Y., Rose, J.M., 2017. Cultivation of the ribbed mussel (Geukensia demissa) for nutrient bioextraction in an urban estuary. Environ. Sci. Technol. 51, 13311–13318. https://doi.org/10.1021/acs.est.7b02838.

Gray, M.W., Pinton, D., Canestrelli, A., Dix, N., Marcum, P., Kimbro, D., Grizzle, R., 2021. Beyond residence time: quantifying factors that drive the spatially explicit filtration Services of an Abundant Native Oyster Population. Estuar. Coasts 45, 1343–1360. https://doi.org/10.1007/s12237-021-01017-x.

Hladik, C., Schalles, J., Alber, M., 2013. Salt marsh elevation and habitat mapping using hyperspectral and LIDAR data. Remote Sens. Environ. 139, 318–330. https://doi.org/10.1016/j.rse.2013.08.003.

Jordan, T.E., Valiela, I., 1982. A nitrogen budget of the ribbed mussel, Geukensia demissa, and its significance in nitrogen flow in a New England salt marsh. Limnol. Oceanogr. 27, 75–90. https://doi.org/10.4319/lo.1982.27.1.0075.

Julien, A.R., 2018. Quantifying the demographics, habitat characteristics, and foundation species role of the ribbed mussel (Geukensia demissa) in South Carolina Salt Marshes. College of Charleston. https://www.proquest.com/dissertations-theses/quantifying-demographics-habitat-characteristics/docview/2066752927/se-2.

Kemp, W.M., Boynton, W.R., Adolf, J.E., Boesch, D.F., Boicourt, W.C., Brush, G., Cornwell, J.C., Fisher, T.R., Glibert, P.M., Hagy, J.D., Harding, L.W., Houde, E.D., Kimmel, D.G.,

Miller, W.D., Newell, R.I.E., Roman, M.R., Smith, E.M., Stevenson, J.C., 2005. Eutrophication of Chesapeake Bay: historical trends and ecological interactions. Mar. Ecol. Prog. Ser. 303, 1–29. https://doi.org/10.3354/meps303001.

Kneib, R.T., Weeks, C.A., 1990. Intertidal distribution and feeding habits of the mud crab, Eurytium limosum. Estuaries 13, 462–468. https://doi.org/10.2307/1351790.

Kravchenko, V.V., 2009. A representation for solutions of the sturm-liouville equation. Front. Math. 2009, 75–91. https://doi.org/10.1007/978-3-0346-0004-0_7.

Kreeger, D., Cole, P., Bushek, D., Kraeuter, J., Adkins, J., 2011. Marine Bivalve Shellfish Conservation Priorities for the Delaware Estuary. Partnership for the Delaware Estuary (PDE) PDE Report.

Kuenzler, E.J., 1961. Structure and energy flow of a mussel population in a Georgia salt marsh. Limnol. Oceanogr. 6, 191–204. https://doi.org/10.4319/lo.1961.6.2.0191.

Leonard, G.H., Levine, J.M., Schmidt, P.R., Bertness, M.D., 1998. Flow-driven variation in intertidal community structure in a Maine estuary. Ecology 79, 1395–1411. https://doi.org/10.1890/0012-9658(1998)079[1395:FDVIIC]2.0.CO;2.

Li, X., Bellerby, R., Craft, C., Widney, S.E., 2018. Coastal wetland loss, consequences, and challenges for restoration. Anthropocene Coasts 1, 1–15. https://doi.org/10.1139/anc-2017-0001.

Lin, J., 1989. Importance of location in the salt marsh and clump size on growth of ribbed mussels. J. Exp. Mar. Biol. Ecol. 128, 75–86. https://doi.org/10.1016/0022-0981(89)90093-2.

Lowe, D.G., 2004. Distinctive image features from scale-invariant keypoints. Int. J. Comput. Vis. 60, 91–110.

Mandlburger, G., Pfennigbauer, M., Riegl, U., Haring, A., Wieser, M., Glira, P., Winiwarter, L., 2015. Complementing airborne laser bathymetry with UAV-based lidar for capturing alluvial landscapes. Remote Sens. Agric. Ecosyst. Hydrol. XVII 9637, 96370A. https://doi.org/10.1117/12.2194779.

Meng, X., Shang, N., Zhang, X., Li, C., Zhao, K., Qiu, X., Weeks, E., 2017. Photogrammetric UAV mapping of terrain under dense coastal vegetation: an object-oriented classification ensemble algorithm for classification and terrain correction. Remote Sens. 9, 1187. https://doi.org/10.3390/rs9111187.

Moody, J., Kreeger, D., 2020. Ribbed mussel (Geukensia demissa) filtration services are driven by seasonal temperature and site-specific seston variability. J. Exp. Mar. Biol. Ecol. 522, 151237. https://doi.org/10.1016/j.jembe.2019.151237.

Morris, J.T., Sundareshwar, P.V., Nietch, C.T., Kjerfve, B., Cahoon, D.R., 2002. Responses of coastal wetlands to rising sea level. Ecology 83, 2869–2877.

Nardin, W., Leathers, J., Vona, I., 2021. Integrating oyster castles into living shorelines to promote coastal bays resilience to sea level rise. Earth Space Sci. Open Arch. 3. https://doi.org/10.1002/essoar.10509555.1.

Nicholls, R.J., Wong, P.P., Burkett, V., Codignotto, J., Hay, J., McLean, R., Ragoonaden, S., Woodroffe, C.D., Abuodha, P.A.O., Arblaster, J., 2007. Coastal Systems and Low-lying Areas.

Pennings, S.C., Bertness, M.D., 2001. Salt marsh communities. Mar. Community Ecol. 11, 289–316.

Peteet, D.M., Nichols, J., Kenna, T., Chang, C., Browne, J., Reza, M., Kovari, S., Liberman, L., Stern-Protz, S., 2018. Sediment starvation destroys New York City marshes' resistance to sea level rise. Proc. Natl. Acad. Sci. 115, 10281–10286. https://doi.org/10.1073/pnas.1715392115.

Pinton, D., Canestrelli, A., Fantuzzi, L., 2020a. A UAV-based dye-tracking technique to measure surface velocities over tidal channels and salt marshes. J. Mar. Sci. Eng. 8, 364. https://doi.org/10.3390/JMSE8050364.

Pinton, D., Canestrelli, A., Wilkinson, B., Ifju, P., Ortega, A., 2021. Estimating ground elevation and vegetation characteristics in coastal salt marshes using uav-based lidar and digital aerial photogrammetry. Remote Sens. 13, 4506. https://doi.org/10.3390/rs13224506.

Pinton, D., Canestrelli, A., Wilkinson, B., Ifju, P., Ortega, A., 2020b. A new algorithm for estimating ground elevation and vegetation characteristics in coastal salt marshes from high-resolution UAV-based LiDAR point clouds. Earth Surf. Process. Landf. 45, 3687–3701. https://doi.org/10.1002/esp.4992.

Pinton, D., Canestrelli, A., Xu, S.Z., 2022. Managing dyke retreat: importance of century-scale channel network evolution on storm surge modification over salt marshes under rising sea levels. Earth Surf. Process. Landf. https://doi.org/10.1002/esp.5521 n/a.

Reed, D.J., 1995. The response of coastal marshes to sea-level rise: survival or submergence? Earth Surf. Process. Landf. 20, 39–48. https://doi.org/10.1002/esp.3290200105.

Ridge, J.T., Rodriguez, A.B., Joel Fodrie, F., Lindquist, N.L., Brodeur, M.C., Coleman, S.E., Grabowski, J.H., Theuerkauf, E.J., 2015. Maximizing oyster-reef growth supports green infrastructure with accelerating sea-level rise. Sci. Rep. 5, 1–8. https://doi.org/10.1038/srep14785.

Schalles, J.F., Hladik, C.M., Lynes, A.A., Pennings, S.C., 2013. Landscape estimates of habitat types, plant biomass, and invertebrate densities in a Georgia salt marsh. Oceanography 26, 88–97. https://doi.org/10.5670/oceanog.2013.50.

Schmid, K.A., Hadley, B.C., Wijekoon, N., 2011. Vertical accuracy and use of topographic LIDAR data in coastal marshes. J. Coast. Res. 27, 116–132. https://doi.org/10.2112/JCOASTRES-D-10-00188.1.

Smith, J.M., Frey, R.W., 1985. Biodeposition by the ribbed mussel geukensia demissa in a salt marsh, Sapelo Island, Georgia. SEPM J. Sediment. Res. 55, 817–828. https://doi.org/10.1306/212f880f-2b24-11d7-8648000102c1865d.

Stagg, C.L., Mendelssohn, I.A., 2011. Controls on resilience and stability in a sediment-subsidized salt marsh. Ecol. Appl. 21, 1731–1744. https://doi.org/10.1890/09-2128.1.

Stiven, A.E., Gardner, S.A., 1992. Population processes in the ribbed mussel Geukensia demissa (Dillwyn) in a North Carolina salt marsh tidal gradient: spatial pattern, predation, growth and mortality. J. Exp. Mar. Biol. Ecol. 160, 81–102. https://doi.org/10.1016/0022-0981(92)90112-N.

Story, M., Congalton, R.G., 1986. Remote sensing brief accuracy assessment: a user's perspective. Photogramm. Eng. Remote. Sens. 52, 397–399.

Wang, D., Xin, X., Shao, Q., Brolly, M., Zhu, Z., Chen, J., 2017. Modeling aboveground biomass in hulunber grassland ecosystem by using unmanned aerial vehicle discrete lidar. Sensors (Switzerland) 17, 1–19. https://doi.org/10.3390/s17010180.

Warren, R.S., Fell, P.E., Rozsa, R., Brawley, A.H., Orsted, A.C., Olson, E.T., Swamy, V., Niering, W.A., 2002. Salt marsh restoration in Connecticut: 20 years of science and management. Restor. Ecol. 10, 497–513. https://doi.org/10.1046/j.1526-100X.2002.01031.x.

Wiegert, R.G., Chalmers, A.G., Randerson, P.F., 1983. Productivity gradients in salt marshes: the response of spartina alterniflora to experimentally manipulated soil water movement. Oikos 41, 1. https://doi.org/10.2307/3544339.

Will, R., Doss, T., Bowers, J., 2012. Ribbed mussels as water filters to clean Jamaica Bay. Water Resour. Impact 14, 15–17.

Wright, R.T., Coffin, R.B., Ersing, C.P., Pearson, D., 1982. Field and laboratory measurements of bivalve filtration of natural marine bacterioplankton. Limnol. Oceanogr. 27, 91–98. https://doi.org/10.4319/lo.1982.27.1.0091.